Impact of terrestrial biosphere on the atmospheric CO₂ concentration across Termination V

Gabriel Hes[1,4], María *F.* Sánchez Goñi[2,4], Nathaelle Bouttes[3]

[1]Département de Géosciences, École Normale Supérieure, PSL Université, Paris, France

5   [2]Ecole Pratique des Hautes Etudes (EPHE), PSL University, Allée Geoffroy Saint-Hilaire Bât. 18N, 33615 Pessac cedex, France

[3]Laboratoire des Sciences du Climat et de l'environnement, LSCE/IPSL, CEA-CNRS-UVSQ-Université Paris Saclay, F91-198, Gif sur Yvette, France

[4]Université de Bordeaux, UMR CNRS 5805 EPOC, Allée Geoffroy Saint-Hilaire Bât. 18N, 33615 Pessac cedex, France

Correspondence to: Gabriel Hes (gabriel.hes@ens.fr)

Abstract. Among the 100kyr climatic cycles of the late Pleistocene, Termination V (TV, ~[404-433] kyr BP), the fifth last deglaciation, stands out for its minimum in astronomical forcing associated paradoxically with maxima in sea level, Antarctic temperature and atmospheric CO₂ concentration. However, the driving mechanisms explaining TV remain only partially

15   understood. For instance, climate models cannot fully represent the atmospheric CO₂ variation observed in paleoclimate data. Aside from essential oceanic circulation processes, there is increasing evidence that terrestrial biosphere may have played a key role in the global carbon cycle. This study proposes a three-step integrated approach, combining regional and global vegetation records with modeling results, to unveil the evolution of terrestrial biosphere and its contribution to the carbon cycle during TV. First, we provide a new high resolution (~700 years) deep-sea pollen record from the Gulf of Cadiz (Site U1386,

20   36°49.680 N; 7°45.320 W) for TV, which shows a moderate expansion of the Mediterranean forest. We then construct the first global forest pollen database for this period. Our compilation features distinct evolutions for different types of forest, highlighting a strong development of temperate and boreal forest which may have delayed the atmospheric CO₂ increase during TV. Finally, the direct comparison of global simulated forests (iLOVECLIM model) to our pollen database reveals consistent forest evolutions despite model biases, thereby supporting a CO₂ mitigation by high latitude forests of the northern hemisphere.

1. Introduction

Among the five major short-term carbon reservoirs of the climate system (ocean, atmosphere, terrestrial biosphere, surface sediments, permafrost), terrestrial biosphere (including vegetation and soils) is considered as an essential component of current

30   anthropogenic climate change mitigation strategies (Harris, et al., 2021, Shukla, et al., 2019). Yet, natural land sinks are also marked by large internal climate variability resulting in uncertainties on the global carbon budget (Loughran, et al. 2021). In

this respect, the study of past climate changes and associated terrestrial biosphere responses remains crucial to reduce uncertainty related to Earth's sensitivity to climate forcings (Overpeck et al., 2003; Masson-Delmotte et al., 2021). Paleoenvironmental research also allows us to investigate terrestrial biosphere feedbacks on the climate on multi-millennial

35 timescales (Overpeck et al, 2003). While extensive studies cover the last glacial cycle (Hoogakker et al. 2016) and the Holocene (Bartlein et al. 2010), there are no global descriptions of terrestrial biosphere for older periods of the Quaternary marked by different climatic boundary conditions.

Termination V (TV, ~[433-404] kyr BP), the fifth last deglaciation, corresponding to the transition between Marine Isotopic

40 Stage (MIS) 12 and MIS11 (Lisiecki et Raymo 2005), embodies complex multi-scale mechanisms. Berger and Wefer (2003) refer to the "Stage-11 paradox" in the following terms: "The amplitude of climate variation is at maximum in the vicinity of Stage 11, at the very time when astronomical forcing is at minimum." Such a conflicting observation emphasizes on the necessity to address this problem within the framework of the entire climate system (cryosphere, ocean, atmosphere, biosphere) together with the Milankovitch theory (Berger and Wefer, 2003). It also highlights the relevance of MIS 11 as an astronomical

45 analog of the present Holocene interglacial (MIS1) featuring low eccentricity (Loutre and Berger, 2003; Berger and Wefer, 2003).

Parallel to the Stage-11 paradox, TV marks a change within the carbon cycle of the 100-kyr climate cycles. As of MIS11, younger interglacials are characterized by higher atmospheric CO_2 concentrations (by about 40 ppm, Lüthi et al. 2008)) and

50 temperatures (Jouzel et al. 2007) compared to older ones. This climatic transition is known as the Mid-Brunhes Event (MBE, ~430 kyr BP). First model simulations by Köhler and Fischer (2006) have shown that low surface temperature in the Southern Ocean together with a reduction of the Atlantic Meridional Overturning Circulation (AMOC) accounted for low atmospheric CO_2 concentrations during pre-MBE interglacials. Simulation experiments also indicate that the pre-MBE period is marked by intense Antarctic Bottom Water (AABW) formation and significant ventilation of the Southern Ocean contributing to carbon

55 storage in the ocean (Yin, 2013). However, recent simulations including a representation of the carbon cycle reveal that the Southern Ocean contribution is too weak to fully explain the carbon uptake during pre-MBE interglacials (Bouttes et al., 2018, 2020). This result suggests a misrepresentation of the magnitude of oceanic processes and/or a lack of crucial mechanisms involved in the carbon cycle such as permafrost or biosphere feedbacks (Bouttes et al., 2018; Barth et al., 2018). Antarctic ice core measurements also indicate that an increase in atmospheric $\delta^{18}O$ during the MBE cannot be fully explained by ocean

60 ventilation (Landais et al., 2010), calling for other explaining mechanisms such as a change in biosphere productivity. Yet, a recent study by Brandon et al (2020) demonstrates that the ocean primary productivity is much weaker than the terrestrial one during TV. Besides, the observed strong increase in carbonate production is not associated with an increase in atmospheric CO_2 as expected but rather with a dampened signal suggesting a compensating process (Brandon et al, 2020).

65   Terrestrial biosphere interacts with global climate through the photosynthesis/respiration feedback involving CO_2 exchanges. So far, the hypothesis of terrestrial biosphere contribution to the change in atmospheric CO_2 across the MBE by change in productivity or geographical distribution remains open. Brandon et al. (2020) suggest that terrestrial biosphere productivity (a major carbon flux component) could have delayed the atmospheric CO_2 increase during TV. However, more regional and global observations of paleo biosphere evolution (Brandon et al., 2020) together with a better representation of

70   biosphere in the coupled climate-vegetation models (Bouttes et al., 2018) are required to identify the impact of the terrestrial biosphere on atmospheric CO_2 concentration across TV. The present study is a first step to fill in this gap, laying the groundwork for a future evaluation of the full carbon cycle. It follows a three-step data-model integrated approach from a regional pollen record analysis to a global assessment of forest evolutions.

1) First, we analyse a new pollen record (U1386) from the Iberian Margin to clarify the vegetation evolution during TV

75   in Southern Iberia. This region is a key location in terms of climate because it is affected by low and high latitude processes.

2) We then provide the first global pollen database for TV in order to understand terrestrial biosphere evolution at global scale. Thanks to our regional U1386 pollen record we separate the temperate and boreal forest evolutions from the Mediterranean one therefore allowing us to capture the spatial variations of terrestrial biosphere evolution across TV.

80   3) Finally, we run model simulations to evaluate the quality of terrestrial biosphere representation by confrontation to the database, and to improve our understanding of the role of terrestrial biosphere in the carbon cycle.

2. Material and methods

2.1 Pollen analysis of IODP site U1386

2.1.1 Regional setting

85   The IODP (Integrated Ocean Drilling Program) site U1386 (36°49.685N, 7°45.321W, 561 meter water depth) was drilled in 2011 during the Mediterranean Outflow Expedition n°339.The site is located in the Faro Drift (Fig. 1), on the upper slope of the Iberian margin (Gulf of Cadiz). As of today, no full record of TV exists for southwestern Iberia. While Site MD01-2447 only describes temperate forests in northern Iberia (Desprat et al., 2005), South Iberian Mediterranean forest evolution remains partially unknown because of a sedimentary hiatus at Site U1385 (Oliveira et al., 2016). U1386 sequence covers a quasi-

90   continuous period from Late Miocene to Holocene (Stow et al., 2013) crossing hemipelagite, turbidite and contourite depositional systems. The core section of interest for TV (Unit IA) is embedded in a unique contourite structure shaped by the historical variations of the Mediterranean Outflow Water (MOW) originating from the Strait of Gibraltar. The local lithology is composed of nannofossil muds, calcareous silty muds and silty bioclastic sands with a dominance of silty muds (Stow et al., 2013). The size of the pollen grains (10-100 μm) belong to the clay fraction and a recent study has shown that fine sediment

95   fraction, including pollen, found on site U1386 essentially originates from the Guadalquivir river although the Guadiana estuary is geographically closer to the site (Moal-Darrigade et al. (2021). Besides, modern pollen samples from the Southern

Iberian margin deep-sea floor have proven to accurately represent the vegetation of the adjacent continent (Naughton et al., 2007; Morales-Molino et al., 2020). Therefore, the pollen record from site U1386 reflects the evolution of the regional vegetation. This vegetation is at present dominated by the Mediterranean vegetation across the Guadalquivir watershed.

100 Deciduous oaks are found at middle elevation while evergreen oaks, olive trees, *Pistacia, Phillyrea* and rockroses (*Cistus*) dominate the lower elevations (Castro et al., 1997). The present-day climate of the South-Iberian Peninsula is directly controlled by the North Atlantic pressure systems dominated by cyclonic cells modulated by the North Atlantic Oscillation (NAO) in winter and by the Azores subtropical high during summer (Lionello et al., 2006). These strong seasonal atmospheric patterns result in mild winters and hot and dry summers (Peinado-Lorca and Martínez-Parras, 1987).

105
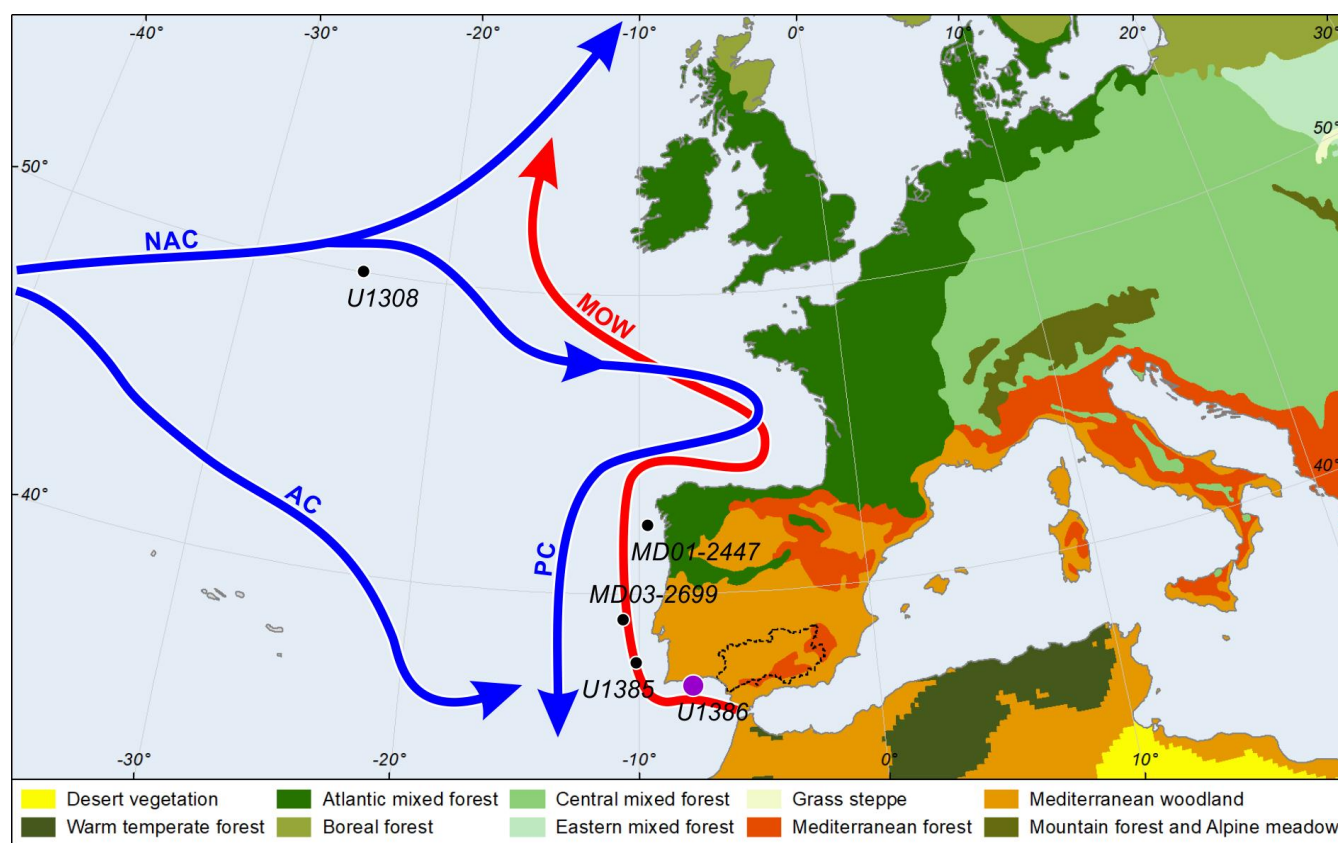
Figure 1: Study area featuring main ocean currents (arrows), vegetation (shading) and sediment cores (dots). Atlantic currents are shown in blue (North Atlantic Current: NAC, Atlantic Current: AC, Portuguese Current: PC) and the Mediterranean Outflow Water (MOW) in red. Colour shading indicates the modern vegetation distribution in Western and Central Europe. Sediment cores are marked by black dots. The
110 present pollen record originates from Site U1386 (purple dot). The Guadalquivir watershed is delimited by a dotted black line. Courtesy of Vincent Hanquiez

2.1.2 Experimental setup

A total of 42 pollen samples from Site U1386, spanning about 7 meters between 138-145 corrected meter composite
115   depth (cmcd), were analysed. The composite core was sampled approximately every 12 cm between 139.81 and 143.39 cmcd
and more loosely on the edges of the sequence (~50cm). Each sample was prepared for pollen analysis following the standard
palynological procedure for marine samples in use at UMR EPOC, University of Bordeaux
(https://ludovicdevaux.wixsite.com/ephe-paleoclimat/about-the-lab). First, a coarse-sieving (150 μm mesh) allowed the
separation of sediments from the finer elements including pollen, spores and dinoflagellates. The resulting fraction was treated
120   with gradually increasing concentrations of HCl and HF to remove carbonates and silicates, respectively, then sieved through
a finer mesh (<10 μm). Known quantities of *Lycopodium* spores were added to the residue to allow reconstruction of absolute
pollen concentrations. Finally, the sample was mounted on a glass slide in glycerol, a mobile medium enabling pollen grain
rotation during observation. Pollen identification was performed at 400× and 1000× magnifications with a Zeiss AXIO Imager
A1 microscope.

125   In order to obtain a reliable representation of the sample composition, at least 100 terrestrial pollen among which 20
different morphotypes excluding *Pinus*, aquatics and spores were counted. The more pollen counted, the better our
concentration estimates are. Rull (1987) shows that a pollen sum of 200 grains is sufficient to produce reliable estimates.
Indeed, for higher values there are no significant variations in the confidence interval width. The 100 grains threshold is a good
compromise for it yields a variation of only ca. 1 % using the multinomial distribution (Maher Jr, 1981) while it reduces the
130   experimental worktime. Changes in pollen percentages detected in our core are therefore significant even considering the 0.95
confidence limits. Counting results are expressed as pollen percentages calculated against the main sum (which discards *Pinus*)
for terrestrial taxa, against the main sum plus *Pinus* for the *Pinus* taxon and against the total sum (Pollen+spores
+indeterminables+unknowns) for the aquatic pollen and spores. Such a distinction avoids flattening of the pollen signal by the
overrepresented *Pinus* in marine sediments (Heusser and Balsam, 1977).

135   Each counted pollen was assigned to an ecological group representative of specific climate conditions. Here we define
six different ecological groups relevant for the Iberian vegetation following previous studies on European vegetation (Polunin
and Walters, 1985). The Mediterranean taxa group (MTss) defined by typical sclerophyllous Mediterranean taxa (*Cistus,
Fraxinus ornus*-type*, Olea, Phillyrea, Pistacia, Quercus* evergreen-type, *Coriaria myrtifolia* and *Quercus* suber-type). This
group indicates a seasonal climate with cool and wet winters and hot and dry summers (Polunin and Walters, 1985, Van Campo,
140   1984). The Mediterranean Forest (MF) is a broader group including the Mediterranean taxa group together with all temperate
and moisture-loving tree and shrub taxa excluding *Pinus, Cedrus, Hippophae, Hemianthemum* and *Cupressaceae* (*Acer, Alnus,
Betula, Carpinus, Corylus, Fagus, Fraxinus* excelsior-type, *Hedera helix, Ilex, Myrica, Populus, , Quercus* deciduous-type,
Rhus-type, *Salix, Tilia, Ulex*-type, *Ulmus* and *Vitis*). The Pioneer group encompasses all plant species able to rapidly colonize
an ecosystem with moderate increase in temperature and precipitation and poor-nutrient soils (*Betula, Cupressacaea,*
145   *Hippophäe*). The Semi-Desert (SD) group is composed of Amaranthaceae-Chenopodiaceae, *Ephedra distachya*-type, *Ephedra*

fragilis-type and *Artemisia* (Van Campo, 1984) while Ericaceae and *Calluna*, typical of annual wet climate, form the Heathland group (Polunin and Walters, 1985). Finally, taxa that can be found in multiple climates fall in the Ubiquist group.

2.1.3 From pollen assemblage to vegetation and climate reconstruction

150

Age model: In order to associate the depth of our composite core with a time scale, we use an improved version of the age model by Kaboth et al. (2017). The age correspondence is based on direct visual correlation between the benthic $\delta^{18}O$ record at Site U1386 and the global mean benthic isotope stack LR04 (Lisiecki and Raymo (2005) for which the chronology is well established. We construct our age model by linear interpolation based on Kaboth et al. (2017)'s calibration points (Table S1

155   in the Supplement) and taking into account Moal-Darrigade et al. (2021)'s splice correction (+0.17m on specific cmcd points. The sequence covers a total of about 28 kyr assuming a constant sedimentation rate of 0.2 m.kyr^{-1} (Kaboth et al., 2017) and features a highest resolution of approximately 500 years (Fig. S1 in the Supplement). We estimate the uncertainty on the chronology to be ~1.2 kyr by computing the quadractic sum of the different age error sources (pollen record resolution, $\delta^{18}O$ record resolution) following the methodology by Govin et al. (2012).

160   The onset of Termination V, as other Middle and Upper Pleistocene terminations, is defined by a drop in the benthic foraminifera oxygen isotope ($\delta^{18}O_b$) below the 3.5‰ threshold (McManus et al., 1999). Averaging over the highest and lowest $\delta^{18}O_b$ values (Skinner and Shackleton, 2005; Shackleton et al., 2003) allows us to position the transition 12/11 (i.e. the end of MIS12 glacial period and the beginning of MIS11 interglacial period) at ~428 kyr BP. The same method applied to local $\delta^{18}O_b$ minima and maxima defines the onset of the substages MIS11d at ~422 kyr BP and 11c at ~418 kyr BP (see Fig. 3).

165

Cluster analysis: The pollen diagram (Fig. 2) computed with Psimpoll software (Bennett, 2000) has been divided in a subset of pollen zones defined by the variation of the percentages of at least two pollen taxa with different ecological affinities (Birks and Birks, 1980). This visual interpretation is supported by a hierarchical clustering analysis based on the minimization of the Euclidean distance and constrained by the number of sample depths (chclust in R environment, Juggins (2009)). The resulting

170   dendrogram (Fig. 2, right) defines six pollen zones across TV.

2.2 Global pollen database

2.2.1 Pollen record selection

We conducted an extensive investigation to retrieve the available marine and lacustrine pollen records covering TV.

175   A total of 14 pollen records with variable resolution were compiled at a global scale (see map on Fig. 5b)). Although each pollen record featured varying taxa according to their location, we extracted (or defined and computed when it was lacking)

the arboreal pollen percentage from each pollen assemblage ("Forest proxy" column, Table 1) in order to build a common metric to measure the evolution of forests globally. As marine and large lacustrine sites collect sediments from surrounding watersheds, each pollen record depicts the regional vegetation setting (Bradshaw & Webb III, 1985; Morales-Molino et al, 180 2020). Table 1 summarizes important information for each pollen record.

Site name	Site n°	Lon (°N)	Lat (°E)	Alt (m)	Type	Forest proxy	Grp	Res	References
ICDP5011	1	172,00	67,50	170 bsl	lacustrine	Trees + shrubs	EA	1,7	Melles et al. (2012)
MD01-2447	2	-9,67	42,15	2080 bsl	deep-sea	Atlantic forest (*Picea*)	EA	1,6	Desprat et al. (2005)
ZB13-C2	3	102,33	33,97	3434 asl	lacustrine	Mainly *Quercus*, *Betula*, *Picea*, *Pinus*	EA	0,5	Zhao et al. (2020)
T. Philippon	4	24,33	41,17	40 asl	lacustrine	Temperate forest	EA	1,8	Tzedakis et al. (2006)
Lake Orhid	5	20,72	41,05	693 asl	lacustrine	Temp + Medit forest -*Pinus*	EA	1,8	Wagner et al. (2019)
IODP U1427	6	134.43	35.97	330 bsl	shallow-sea	Temp + Warm Temp + cold conifer	EA	8,9	Hayashi et al. (2021)
IODP U1385	7	-10,12	37,57	2578 bsl	deep-sea	Mediterranean forest	M	1,2	Oliveira et al. (2016)
IODP U1386	8	-7,76	36,83	561 bsl	deep-sea	Mediterranean forest	M	0,7	This study
Funza	9	-74,33	4,83	2550 asl	lacustrine	High plain forest	T	1,5	Torres et al. (2013)
ODP 108-658	10	-18,60	20,70	2275 bsl	deep-sea	Sudanese and Guinean forests	T	5,7	Dupont et al. (1989)
GIK16867-2	11	5,10	-2,20	3890 bsl	deep-sea	Afromontane forest	T	2,3	Dupont et al. (1998)
GIK16415-2	12	-19,10	9,60	3845 bsl	deep-sea	Fern spores	T	5,1	Dupont and Agwu (1992)
Lake Magadi	13	36,27	-1,87	579 asl	lacustrine	Afromontane forest + woodland	T	6,9	Johnson et al. (2016)
MD96-2048	14	34,02	-26,17	660 bsl	shallow-sea	Mountain forest + woodland	SA	7,2	Dupont et al. (2011)

Table 1: Database summary table. Pollen record altitudes (Alt) are given in meters bsl and asl, standing for "below sea level" and "above 185 sea level" respectively. Pollen selected to build the arboreal pollen percentage are described in the Forest proxy column. Each pollen record is allocated to a group (Grp column): SA (South African), T (Tropical), M (Mediterranean) or EA (Euroasian). The penultimate column (Res) features the mean temporal resolution (kyr) of the sequence.

2.2.2 Data analysis

Each pollen record was resampled with a 2-kyr time step in order to build consistent composites. The timestep value 190 was chosen in order to optimize the database resolution and minimize oversampling of coarse resolution records (more than half of pollen records feature a mean resolution below 2 kyr, Table 1). Four record groups were defined according to their main ecological and geographical specificity: South African, Tropical, Mediterranean and Eurasian groups (Table 1). Forest pollen composites were then obtained by averaging the forest pollen percentage for each group (Fig. 5). It should be noted that all groups i) are made of very few records, ii) do not contain the same number of records. As a consequence, it is difficult to 195 compare the composites between them and to estimate a statistical robustness of their signal. However, a sensitivity analysis (not shown) performed on the composites for varying resampling timestep values (between 1 and 4 kyr) revealed no significant change. Besides, as each record has its own chronology (and associated uncertainty), the present analysis only allows to compare long-term trends in the forest pollen signals.

2.3 Model and experimental setup

2.3.1 Model description

We use the three-dimensional Earth system model of intermediate complexity iLOVECLIM, an evolution of the LOVECLIM version 1.2 (Goosse et al., 2010) resolving the carbon cycle (Bouttes et al., 2015). iLOVECLIM includes an ocean module (3°x3°horizontal grid, 20 vertical levels), a simplified atmospheric module (~5.6°x5.6°horizontal grid, on 3 vertical layers), a biogeochemical module (Bouttes et al., 2015, 2020) and a terrestrial biophere module (VECODE, Brovkin et al. (1997). For each terrestrial gridpoint, the vegetation module computes two main Plant Functional Types (PFTs), herbaceous (g) and trees (t), and a desert fraction (d) such that their sum equals 1 (i.e. g+t+d=1). For example, an ice sheet grid point will feature null tree and herbaceous fractions and a desert fraction of 1 (Roche et al, 2007).

2.3.2 Model simulations

Using iLOVECLIM,we have run a long-time experiment covering TV (Degla-V, 436-404 kyr). While the present study focuses on TV, we have also run a simulation of TI (Degla-I, 21-0 kyr) to check consistency with previous studies of the Last Deglaciation (Fig. S6 in the Supplement, Roche et al., 2011). In order to obtain stable initial conditions, a spin-up (stationary) simulation is run over 5 kyr for each experiment (~3 kyr are required to reach an equilibrium in the deep ocean) by fixing the orbital parameters (Berger 1978), the greenhouse gases (CO_2 and CH_4) and an ice sheet model output (Ganopolski and Calov, 2011) at the time of maximum ice sheet (436 kyr BP and 21 kyr BP for Degla-V and Degla-I respectively). The two transient simulations are then run with the forcings (orbital parameters, greenhouse gases and ice sheet), now varying with time.

3. Results

3.1 Pollen record and inferred Southwestern Iberia vegetation and climate

We identify five major pollen zones (Figure 2) corresponding to major shifts in vegetation cover and composition. A summary of the following vegetation description for each pollen zone is provided in Table 2.

The first major zone U1386-1 (~145.1-143.7 cmcd) is dominated by Ubiquists (~30%), SD (~40%) and Pioneer taxa (~20%) while the MF remains low (<10%). The important presence of SD such as Amaranthaceae-Chenopodiaceae, *Ephedra* and *Artemisia* suggests a dry and cold climate consistent with the MIS12 glacial period. The large proportion of Pioneer taxa (mainly *Cuppressaceae*) and low MF further confirms that climate conditions were too harsh for large temperate trees to grow, leaving a shrub-dominated land cover. The end of zone U1386-1 is characterized by a decrease in SD and Pioneer percentages while the Ubiquist proportion increases drastically mainly driven by *Taraxacum* and *Poaceae* expansion. Interestingly, this rapid shift occurs immediately after an extremely high pollen concentration peak (>50000 pollen/cm3, Fig. S2 in the Supplement) highlighting a significant increase in Ubiquist pollen number and a real transition from a SD-dominated assemblage to a Ubiquist-dominated one. Such an important pollen concentration event can be caused by a wide range of

factors including changes in pollen productivity and dispersability, in the source area and in the distance to the sampling site but also in the rate of sediment deposition associated with the sea level increase.

235   The second major zone U1386-2 (~143.7-142.6 cmcd) is characterized by a dominance of Ubiquists (~70%) mainly represented by *Taraxacum* and *Poaceae*. The SD and Pioneer groups are much weaker than in zone U1386-1 (~15% and <10% respectively) while Heathland group grows up to 10% across the zone providing evidence for increasing humidity. We decide to divide zone U1386-2 into two sub-zones (U1386-2a and U1386-2b), considering the emergence of MF taxa (mainly *Olea* and *Pistacia*) at around 143 cmcd. Sub-zone U1386-2a corresponds to a relatively humid climate yet still too mild to bear

240 forest development. However, if sub-zone U1386-2b is as humid as U1386-2a as suggested by the continuous *Isoetes* spores record, it is especially warm enough to allow a strong increase of the Mediterranean forest. Therefore, the low limit of this sub-zone defines the onset of the terrestrial interglacial (Sánchez Goñi et al., 1999; Shackleton et al., 2003). The overrun of the 20% threshold in MF at the high limit of the sub-zone depicts a settled and developing Mediterranean forest (Sánchez Goñi et al. 2016), indicating atmospheric warmth and moisture availability but also a seasonal climate.

245
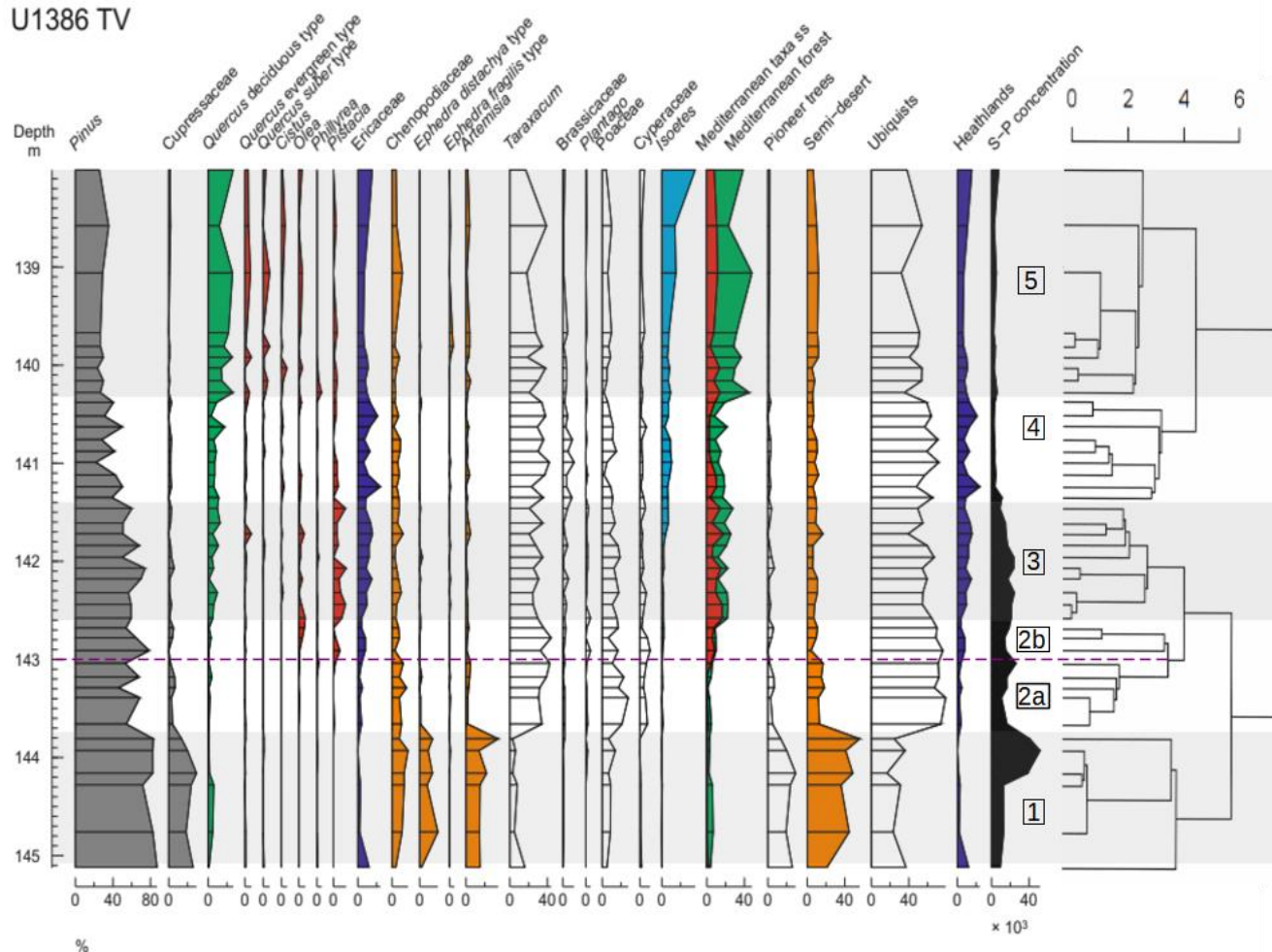
Figure 2: Pollen percentage diagram of selected morphotypes and ecological groups at Site U1386 versus depth (cmcd). Sporo-pollen concentrations (number.cm^{-3}) are displayed on the last curve on the right and alternating gray/white shading with corresponding numbers

250   indicate pollen zones. The dendrogram showing the results from the hierarchical clustering analysis is represented on the right. The purple dashed line indicates the onset of the terrestrial interglacial. The same colors are used for the ecological groups and the main morphotype components thereof.

The MF (mainly *Quercus* deciduous and *Pistacia*) and the Ubiquist groups are still present throughout Zone U1386-

255   3 (~142.6-141.4 cmcd), oscillating around 20% and 50% respectively, indicating continuous development of forested area. Zone U1386-3 is also characterized by a higher development of Heathlands (10 to 20%) than in zone U1386-2 mainly driven by increased Ericaceae proportions. Moreover, the significant emergence of *Isoetes* spores (~10%) starting around 142 cmcd is a strong signal for deglaciation. In fact, *Isoetes* grows in marshlands, which gradually expand during an increase in

precipitation associated with the transition between glacial and interglacial climates (Sánchez Goñi et al., 1999). The end of

260 Zone U1386-3 is marked by a strong drop in pollen concentration (Fig. S2 in the Supplement), which could be caused by a sea level rise, providing further evidence for ice sheet collapse during the transition between Zone U1386-3 and U1386-4. The beginning of Zone U1386-4 (~141.4-140.3 cmcd) is defined by a strong decrease of the Heathland group (down to less than 10%) mainly owing to a decline in Ericaceae. Yet, Zone U1386-4 features one of the highest Ericaceae percentage of the whole sequence.

265

Pollen zone (basal depth in cmcd, age in ka)	Duration of interval (kyr) (number of samples)	Pollen signature	Vegetation interpretation
U1386-1 (145.1, 433.6)	5 (6)	Significant dominance of non-arboreal taxa composed of semi-desert (SD, ~40%) plants such as Amaranthaceae-Chenopodiaceae, *Ephedra distachya* type and *Artemisia* and Ubiquist (~30%) plants including Poaceae and *Taraxacum*. The only few tree taxa are *Pinus* and Cupressaceae (Pioneer group ~20%) while the Mediterranean forest (MF) and heathland group frequencies remain very low.	Dry shrub-type vegetation with *Pinus* forests
U1386-2a (143.7, 428.6)	2.1 (3)	Decrease in SD and pioneer percentages at the beginning of the zone while the Ubiquist proportion increases drastically (mainly driven by *Taraxacum*, Poaceae and Cyperaceae expansion) highlighting a transition from a SD-dominated assemblage to a ubiquist-dominated one (~70%).	Shrub-dominated land cover with vanishing pioneer tree coverage.
U1386-2b (143.2, 426.5)	2.9 (5)	Rise of Mediterranean taxa including *Olea* and *Pistachia*. Continued dominance of ubiquist taxa.	First occurences of Mediterranean taxa.
U1386-3 (142.6, 423.6)	5 (10)	Slightly increasing Mediterranean forest abundance (>20%) due to the appearance of *Quercus* deciduous-type and the continuous presence of *Pistachia* although marked by large fluctuations. Higher heathland frequency (10 to 20%) driven by the development of Ericaceae. Dominance of ubiquist taxa oscillating around 60%. Increase of *Isoetes* spores at the end of the zone.	First step of Mediterranean forest expansion coinciding with development of Ericaceae and heathland
U1386-4 (141.5, 418.6)	5 (9)	Quasi-absence of Mediterranean taxa including *Olea*, *Pistachia*, *Cistus*, *Quercus* suber-type and *Quercus* evergreen accounts for a reduced expansion of the MF.	Coexisting heathland and Mediterranean forest vegetation
U1386-5 (140.3, 413.2)	9 (9)	Surge of the MF frequency (up to 40%) mainly owing to both increasing *Quercus* deciduous type and MTss taxa) accompanied by a slight decrease in Ubiquist group (down to 35%). Stable low SD percentages while increase in *Isoetes* spores abundance across the zone	Second step of Mediterranean forest expansion

Table 2: Description and interpretation of the TV pollen record at Site U1386.

The onset of U1386-4 is also marked by an increase in Ubiquist group (up to 70%) while the SD group remains at relatively low levels (~10%), changes which could be attributed to a wetter or warmer climate. However, the MF also decreases

270 and remains low (mostly below 20%) throughout the period while *Isoetes* spores grow over 10%. These variations describe a decreasing atmospheric temperature and still wet conditions. Besides, the very stable pollen concentration (~4000 pollen/cm3, Fig. S2 in the Supplement) reflects an absence of major changes in the deposition factors, which are mainly related to sea level and oceanic currents. Therefore, we hypothesize that atmospheric temperature decrease is the major environmental change influencing vegetation in Zone U1386-4.

275 The transition to Zone U1386-5 (140.3-138 cmcd) is characterized by a surge of the MF group (up to 40% mainly owing to increasing *Quercus* deciduous) and a decrease in Ubiquist group (down to 35%) while SD group and *Isoetes* spores

remain relatively constant and MTss pollen percentages increase. As pollen concentrations do not vary much over this period, we can infer a strong expansion of the Mediterranean forest. In Zone U1386-5, the MF and Ubiquist group percentages follow opposed variations while the other groups remain relatively stable, depicting variations in the percentage of forested and open vegetation land cover. A second MF peak is reached around 139 cmcd, suggesting a stable development of the Mediterranean forest that indicates the warmest climate of the considered interval and wet winter conditions.

3.2 South-Iberian terrestrial biosphere evolution across TV

We now interpret U1386 pollen record in a temporal framework by comparing reconstructed vegetation to other climate indices (Fig. 3). Given that all proxies originate from the same sediment core, a direct comparison is possible without chronology issues.

The first important result is that the terrestrial interglacial (~424 kyr BP, >20% MF) begins ~4000 years after the marine isotopic interglacial (~428 kyr BP, $\delta^{18}O_b$). The onset of MIS11e is characterized by a minimum of precession and increasing insolation at 65 °N responsible for significant decrease of the ice volume visible in the drop of $\delta^{18}O_b$. This important melting event is also supported by surrounding records (Fig. S3 in the Supplement). The increase in the Si/Sr values from site U1308 in the central North Atlantic (Fig. 1) indicates the presence of Ice Rafted Debris (IRD) carried by icebergs originating from the North American ice caps while the increase of $C_{37:4}$ values from an Iberian margin core (MD03-2699) located slightly North from U1386 (39 °N, Fig. 1) depicts freshwater pulses in the southwestern Iberian margin at the end of MIS 12 (Fig. S3 in the Supplement). Such a cold water input in the northern North Atlantic from the end of MIS12 until the beginning of MIS11e results in a weakening of AMOC highlighted by low $\delta^{13}C$ values, a decrease in sea surface temperature supported by the high abundance of *Neogloboquadrina pachyderma* (s), and cold and dry conditions in Southwestern Iberia revealed by the SD taxa expansion. The onset of MIS11e coincides with a severe drop of SD taxa and a rise in Ubiquists. These opposite evolutions suggest an increase in atmospheric humidity. However, the MF only develops several millennia later, towards the end of MIS11e. This first moderate forest development is driven by the growth in sclerophyllous Mediterranean taxa (MTss) particularly adapted to the low precession-induced high seasonality. The present U1386 high resolution pollen record allows us to reposition the beginning of the SINES terrestrial interglacial - previously defined by Oliveira et al. (2016) - at ~424 kyr BP about 4 kyr after the onset of the marine interglacial (MIS11).

Termination V further stands out owing to a two-step forest development, absent from more recent terminations (see Figure 5 in Sánchez Goñi et al. (2018)). The first increase in Mediterranean forest (~424 kyr BP) is relatively limited (~20%) compared the second (~40%) which is more representative of a true forest expansion in the South Iberian Peninsula. The reduced Mediterranean forest develops across MIS11d synchronously with heavier $\delta^{18}O_b$, suggesting a temporary ice sheet growth. The increasing obliquity causes enhanced insolation seasonality with higher precipitations in winter while high precession results in increased summer precipitations in our region (Bosmans et al., 2015), explaining the growth of Heathland taxa which require year-round precipitation. The second forest development starting around 414 kyr BP occurs with slightly different orbital parameter settings: high obliquity but decreasing precession such that the highest MF expansion coincides

with the insolation maximum. A combination of low precession and high obliquity is known to be even more favorable to winter precipitation (Bosmans et al., 2015).
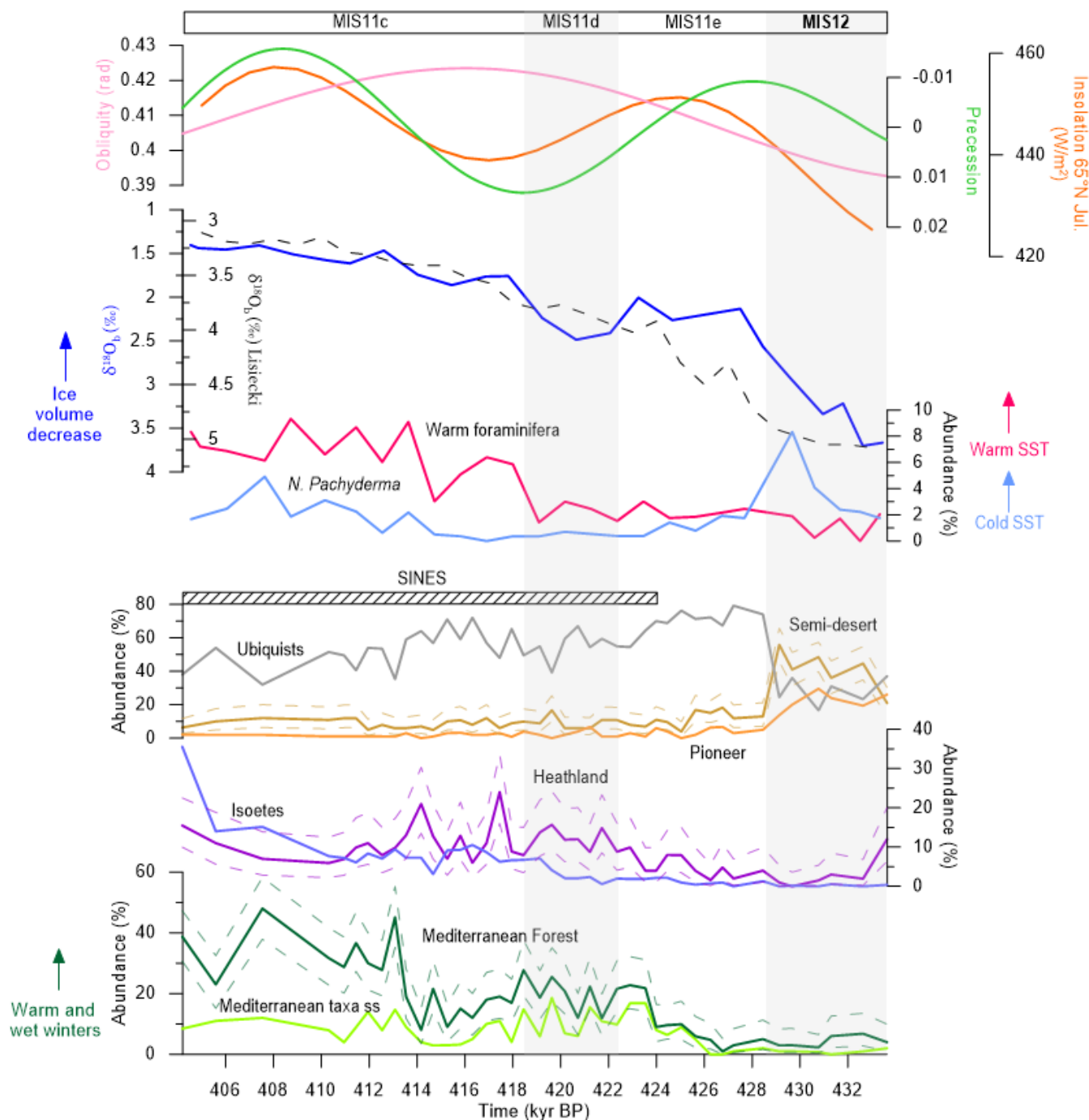
Figure 3: U1386-retrieved environmental indicators. From bottom to top: Pollen percentages (this study), warm and cold foraminifera
315   abundance (Moal-Darrigade et al., 2021), δ18O (from U1386 in blue: Kaboth et al., 2017, and global in black dashed: Lisiecki & Raymo,

2005) and astronomical parameters (source: http://vo.imcce.fr/insola/earth/online/earth/online/index.php). The dashed lines represent the 95% confidence intervals for MF, Heahtland and SD (computed with 'exactci' package, R).

320 Besides, the high abundance of warm foraminifera indicates a warmer ocean than at the beginning of the SINES interglacial. This warming is supported by the reconstructed atmospheric temperature featuring a difference of about 2°C between 424 and 414 kyr BP (Fig. S4 in the Supplement). Such environmental conditions are consistent with a larger growth of the Mediterranean forest. Finally, we observe an abnormal contraction of the MF at the beginning of the MIS11d (~418 kyr BP) which can be explained by the combination of maximum obliquity and precession accounting for low seasonality. This

325 relatively mild and humid climate is however adapted for the development of Ericaceae which is responsible for the peaks in Heathland taxa. Overall, even the highest Mediterranean forest pollen percentages of MIS11 are relatively low in regards to recent interglacials such as MIS1 and MIS5e (see Fig. 5 in Sánchez Goñi et al., 2018), suggesting a moderate development of the terrestrial biosphere in southern Iberia during TV.

330
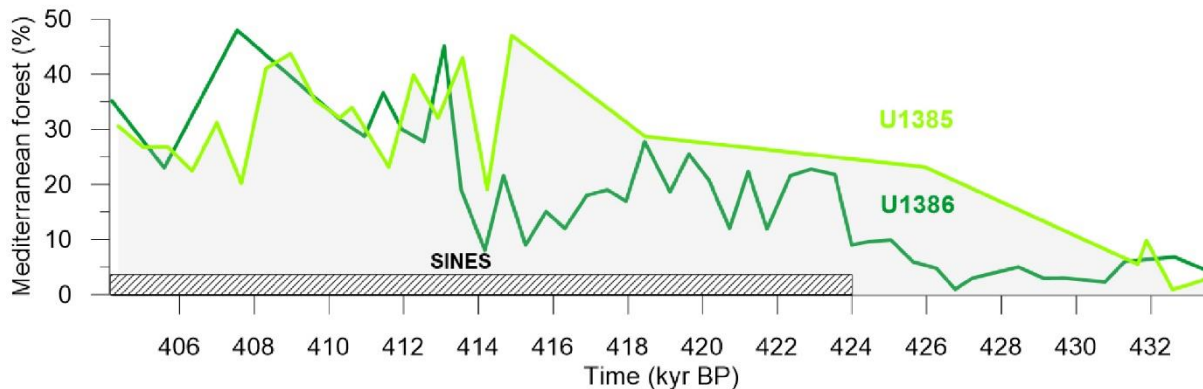
Figure 4: Comparison of Mediterranean forest (%) from U1386 (our study) and U1385 (by Oliveira et al. (2016), see map Fig. 1)

335 Our new high resolution pollen record (U1386) sheds light on the Southern Iberian terrestrial vegetation across TV, a period poorly documented owing to a sedimentary hiatus in the previous IODP site U1385 pollen record (Oliveira et al. (2016)). A comparison of U1386 and U1385 records on Fig. 4 reveals a more complex Mediterranean forest evolution than previously thought. While the overall trend of both series is consistent, we observe a slight shift between U1385 and U1386 over the last part of the sequence (U1385 leading U1386 by about 2 kyr, with a maximum at 415 and 413 kyr respectively (Fig.

340 4), which we attribute to differing age models. The U1386 record allows us to define a more precise onset of the Mediterranean forest at ~424 kyr BP. As previously mentioned, the U1386 record unveils a two-step forest development absent from the

U1385 record, with a first moderate expansion between 424 and 418 kyr BP (onset of the SINES Mediterranean forest phase) and a second larger expansion starting at 414 kyr BP (Fig. 4). Finally, both U1386 and U1385 feature a maximum Mediterranean forest percentage of ~50%, therefore agreeing on a moderate Mediterranean forest development during the

345   SINES forest phase.

3.3 Global terrestrial biosphere evolution across TV

3.3.1 Global pollen composite records

350   In this section, we take a step back from our regional analysis to investigate the evolution of the terrestrial biosphere at a global scale thanks to our new pollen database. Forests are reliable proxies for terrestrial biosphere (Crowley, 1995; Prentice et al., 2011; Brandon et al., 2020). Therefore, we postulate that the evolution of the pollen-based forest percentage is representative of terrestrial biosphere evolution. Fig. 5b) features the pollen record database locations and Fig. 5a) the corresponding forest pollen percentages across TV. At first sight one can notice a large percentage difference between pollen

355   records (see also Fig. S5 in the Supplement), some records averaging around 10% (e.g. ODP 108-658) and others rising over 90% (e.g. Tenaghi Philippon). This reveals strong environmental discrepancies between the sampled regions. Building composites allows us to compare records in presumably similar global climatic conditions to extract information concerning the long term evolution of forests in a specific location.

        The tropical composite features a relatively constant forest pollen percentage (between ~40 and ~65%) across

360   Termination V. However, this constant envelope is marked by variations such as a large drop between 432 and 427 kyr BP followed by an increase until 423 kyr BP. The Mediterranean composite is characterized by a slow increase in forest pollen percentages from 2% at 433 kyr BP to a maximum value of 40% around 409 kyr BP. One must keep in mind that this group is composed of only two observations recording the South Iberian Peninsula forest. This result is in line with the mild development of the Mediterranean forest over Southern Iberia during MIS11 discussed previously in U1386 record. The

365   Eurasian group includes records from very different locations (Tibetan plateau, Siberia, continental Europe, Japanese peninsula). The resulting composite is first marked by a sharp and substantial increase in pollen percentages from 25% at 430 kyr BP to 60% at 423 kyr BP, then by a slow growth peaking at 68% around 411 kyr BP while the last part of the sequence features a slight drop at 407 kyr BP. Finally, the South African forest pollen percentages decrease by over 10% across TV. Overall, the present composite analysis highlights the strong development of temperate and boreal forests at mid- and high-

370   latitude in the northern hemisphere (Eurasian group) between 430 and 423 kyr BP. However, the limited number of pollen records also calls both for more observational data and for climate-vegetation simulations to gain further insight into the global terrestrial biosphere evolution.
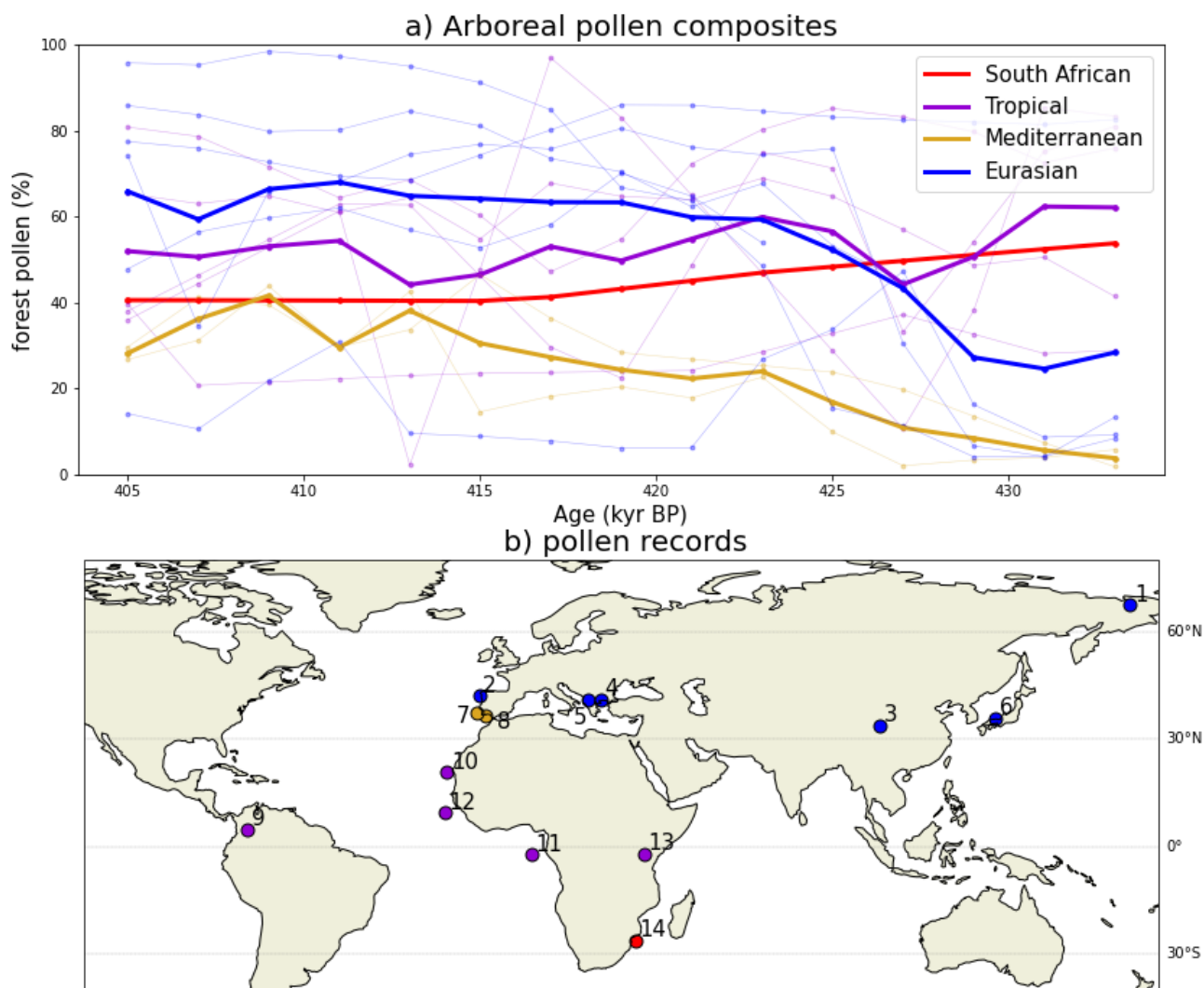
375

Figure 5: Forest pollen records and composites a) and pollen record locations b). Colors refer to the same regional groups in a) and b). In a), pale lines represent the forest pollen records and bold lines the forest pollen composite for each group. The site numbers in b) refer to Table 1.

380 **3.3.2 Model-data comparison**

The iLOVECLIM climate simulation of TV (Degla-V) provides a complementary view to that of the pollen composites, allowing a better evaluation of the forest development and its possible impact on atmospheric CO_2 changes recorded during TV. Figure 6 features the simulated tree fraction (Degla-V) and the forest pollen records at 433 kyr BP (glacial period, Fig. 6a) and 405 kyr BP (end of deglaciation, Fig. 6b). Based on numerous studies on the present-day pollen-vegetation

385   relationships (e.g. Huntley and Birks, 1983; Huntley B. , 1990; Morales-Molino et al., 2020), we assume that pollen forest percentage is a good indicator of the tree fraction.

The absence of simulated tree at high latitudes (>60 °N) at 433 kyr on Fig. 6a) is consistent with the presence of a large ice sheet over North America, Greenland and Siberia during MIS12 (Batchelor et al., 2019). As expected, the high simulated tree fractions are located at lower latitudes and specifically around the Equator. However, there are two important

390   and known model biases concerning simulated tree fractions (Goosse et al., 2010). The model features high Amazon forest along the Eastern, Northern and Western South American coastline, while there is no reason why trees should be absent from inland regions of Northern South America. This can be explained by a tube-like modeled Amazon river hindering moisture fluxes from the river to the atmosphere and resulting in a desert environment in the Tropics. On the African continent, Equatorial forest is shifted to the East with desert-like Sub-Saharan regions. This anomaly derives from a low resolved African

395   monsoon (Goosse et al., 2010).

The forest pollen observations overall support the simulated tree fraction while they also underline the abovementioned model biases both at the onset (Fig. 6a) and the end (Fig. 6b) of TV. The northward gradient of simulated forest fraction over the Iberian Peninsula at 405 kyr BP (Fig. 6a) is consistent with lower forest pollen percentages in Southern Iberia compared to Northern Iberia supporting the idea that temperate forest is more developed than Mediterranean forest at

400   the end of TV. The Balkan and the Tibetan simulated tree fraction (<20%) agrees with the low pollen percentages at 433 kyr BP. The northernmost African record (ODP 108-658) featuring an absent Saharan forest is also well captured by the model both at 433 and 405 kyr BP. However, the model and observations disagree at 433kyr BP over Equatorial Africa where the records describe a strongly rooted forest (forest pollen > 80 %) while the simulated tree fraction is very low, and over South Africa where the model overestimates the forest proportions (for both 433 and 405 kyr BP), thus highlighting the

405   aforementioned model biases. Finally, Japanese, Siberian and the Amazonian simulated forests are relatively consistent with the corresponding pollen percentages.

On Fig. 6c we compute the difference between maps b) and a) in order to cancel out the systematic model biases and to illustrate the forest expansion/retreat over the whole deglaciation (405-433 kyr BP). As two pollen records (ICDP5011 and MD01-2447) do not cover the whole Termination, a second difference map (Fig. 6d, 405-423 kyr BP) complementary to Fig.

410   6c and including all sequences is proposed, although we mainly focus on Fig. 6c to reveal the full deglaciation forest trends. The impact of ice sheet melt is marked by strong forest development north of 60 °N in Siberia, surrounding the Bering Strait (confirmed by ICDP5011 record on a shorter time scale (Fig. 6d)), and at 50 °N over the Northwestern American continent. Model and data agree over Tibet where a slight forest growth is observed and over Japan where the forest remains stable. The simulation underestimates the forest expansion in the Iberian, the Balkan and the Amazonian regions and the forest retreat in

415   Southern Africa. Finally, we observe contrasting results over Tropical Africa. The increasing simulated forest is in line with two West African deep-sea records (ODP 108-658 and GIK16867-2) but disagrees with recorded forest decline on the West (GIK16415-2) and the East (Lake Magadi) adjacent landmasses.
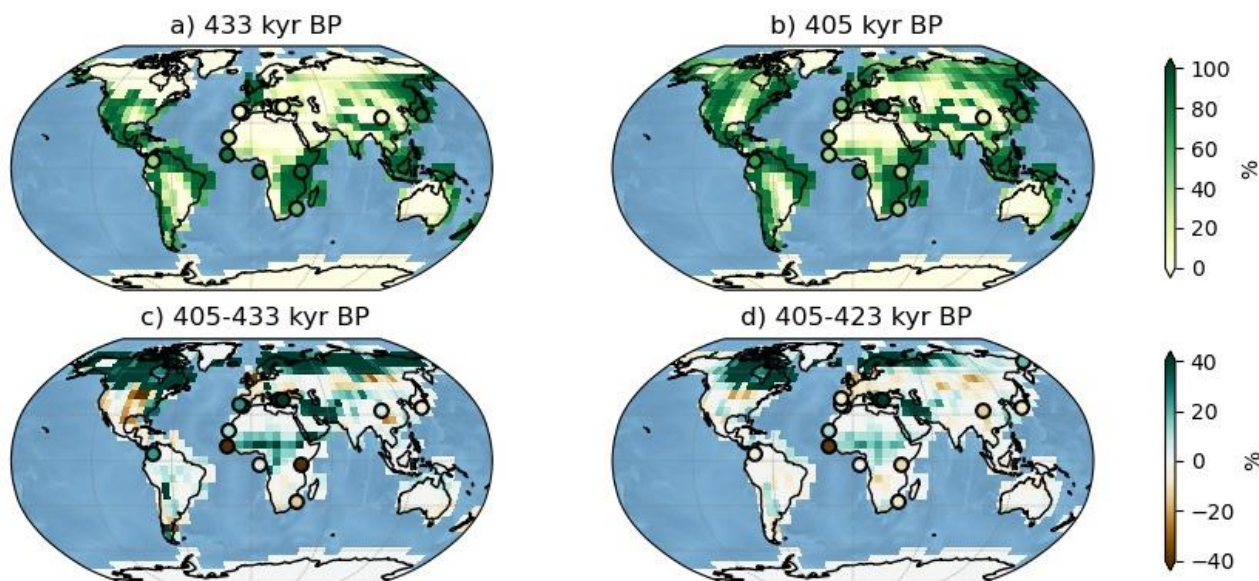
Figure 6: Global comparison of simulated tree fraction (square patches, %) and forest pollen from records (circles, %) at 433 kyr BP (a) and
420   at 405 kyr BP (b). (c) and (d) feature the tree fraction difference between 405 and 433 kyr BP (423 resp.). Pollen record percentages should

be compared to the simulated tree fractions of the closest adjacent land.

4. Discussion

425

Our integrated research approach from regional pollen record analysis to global climate simulation opens for multiple
discussion levels for both the observation and the modelling communities.

4.1 Assessing regional forest development across Termination V

430

In this section, we use Degla-V simulation (in addition to the sparse, yet essential pollen records) to provide a finer temporal
analysis of forest developments for selected regions of the world (Fig. 7). We choose eight regions based on special features
emerging from Fig. 6c: either regional uniform trends (e.g. Siberia) or regional heterogeneous trends (e.g. central Asia). As
already noticed for pollen composites (Fig. 4), we also observe regional discrepancies in the simulated tree fraction. Europe is

characterized by a very weak increase in forest coverage (solid line) consistent with the pollen record average over the second part of the deglaciation (although ~10 points below) but inconsistent during the beginning. Although the observed strong temperate forest development at the onset of TV originates from southern Europe records only, there is nearly no increase in the simulated tree fraction, suggesting a possible misrepresentation of growing conditions. Given the low horizontal resolution of the atmospheric module, we suspect that precipitation inaccuracies might account for the underestimated simulated forest growth. The Mediterranean region features an increasing forest trend both for the simulation and record average, however much weaker in the simulation for similar reasons. Forest expansion reaches a maximum at ~410 kyr BP for the model (resp. ~408 kyr BP for the data) before shrinking at the end of the sequence. For Central Asia and Amazon regions, the simulated tree fraction is relatively constant (~45% and ~60% respectively) and overall in line with the record average. In Tropical Africa, we observe a constant simulated forest growth across TV reaching a maximum of nearly 50% at 410 kyr BP before decreasing. This region is characterized by contrasting pollen record signals. Nonetheless, the record average also features a forest expansion peak synchronous with the simulated one. North America (S) tree fraction remains stable across the termination with increasing trends (East coast) compensating decreasing trends (central North America, see Fig. 6c). The latter is confirmed by the pollen sequence of Valles Caldera in SW North America, which shows a relatively low development of the forest cover with a decreasing trend of *Picea, Abies and Quercus* from 420 to 405 kyr BP (Fawcett et al., 2011). Finally, the two northernmost regions (North America (N) and Siberia) are totally unforested during the MIS12 glacial stage and both highlight a strong forest development during the deglaciation and a peak towards the end. The North American (N) region reaches a peak of 40% at ~409 kyr BP while the Siberian region settles around 50% from 413 kyr BP before decreasing at 408 kyr BP. Despite the lack of precise pollen record to constrain the simulated forest evolution over North America (N), de Vernal et al (2008) find, in a deep-sea sedimentary sequence collected off Greenland, that the highest pollen concentrations of *Picea* over the last 1 million years occurs between 410 and 390 kyr BP, thus supporting the idea of a strong forest expansion in the North America (N) region during TV. Concerning Siberia, the only available record (ICDP5011) features a similar trend but 20 to 30 points above the simulated. We explain such a difference by the variable influence of ice retreat on forests depending on the latitude. The northernmost gridpoints of the region experience a widespread growth (similarly to the ICDP5011 record) because of a net increase in available land whereas southernmost gridpoints are mostly affected by changes in atmospheric temperatures, CO_2 concentrations and precipitation, resulting in lower forest expansion. (see Fig. 6c). Overall, the simulated tree fraction at high latitude in the northern hemisphere show a strong increasing trend (+[40:50]%) over the deglaciation, supporting the argument for a massive boreal and temperate forest development.
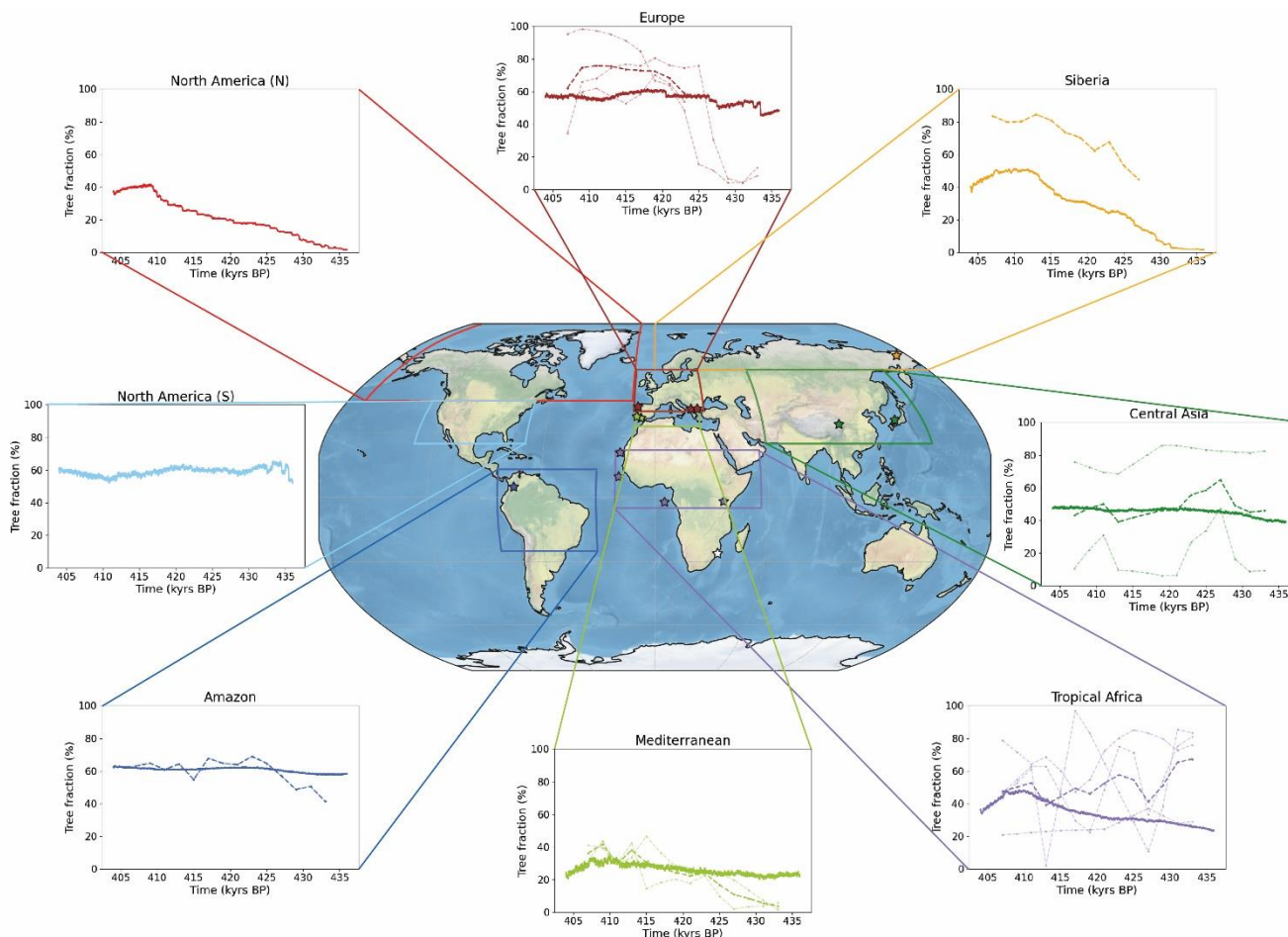
Figure 7: Comparison of simulated tree fraction and forest pollen percentage by region across TV. Each plot shows the simulated tree fraction average (%, solid line) over the corresponding regional box (colored contours) and associated forest pollen record (%, pale dotted line) and record average (%, bold dotted line) when available. Locations of pollen records are marked by colored stars.

4.2. Atmospheric CO₂ mitigation by Eurasian forests

At a global scale, both pollen observations (Eurasian composite on Fig. 5a) and model simulations (North America (N) and Siberia time series on Fig. 7) outline that Termination V is characterized by a strong increase of boreal and temperate forest between ~429 and ~423 kyr BP. We suggest that this result can support recent findings by Brandon et al. (2020). Brandon et al. (2020) show an abrupt increase in the global biosphere productivity from ~429 and ~427 kyr BP resulting in anomalously high values (10 to 30% higher than preindustrial) which would explain the atmospheric CO₂ levelling from ~425 to ~415 kyr BP (Fig. 8). This global biosphere productivity extreme is unique among the last five interglacials, and it is mainly attributed to terrestrial biosphere (Brandon et al. (2020)). With forests as terrestrial productivity indicators, we seek to specify the

geographical origin of such important carbon dioxide mitigation. Among the four pollen composites, the Eurasian region (dashed blue line) features the most important forest expansion (strongest increasing trend, Fig. 8). Besides, this significant

480   development is synchronous with the surge in the productivity signal (429-425 kyr BP). Therefore, we propose that Eurasian forests, including temperate and boreal forests, account for the high terrestrial biosphere productivity and the moderate atmospheric CO_2 values at the beginning of MIS11.
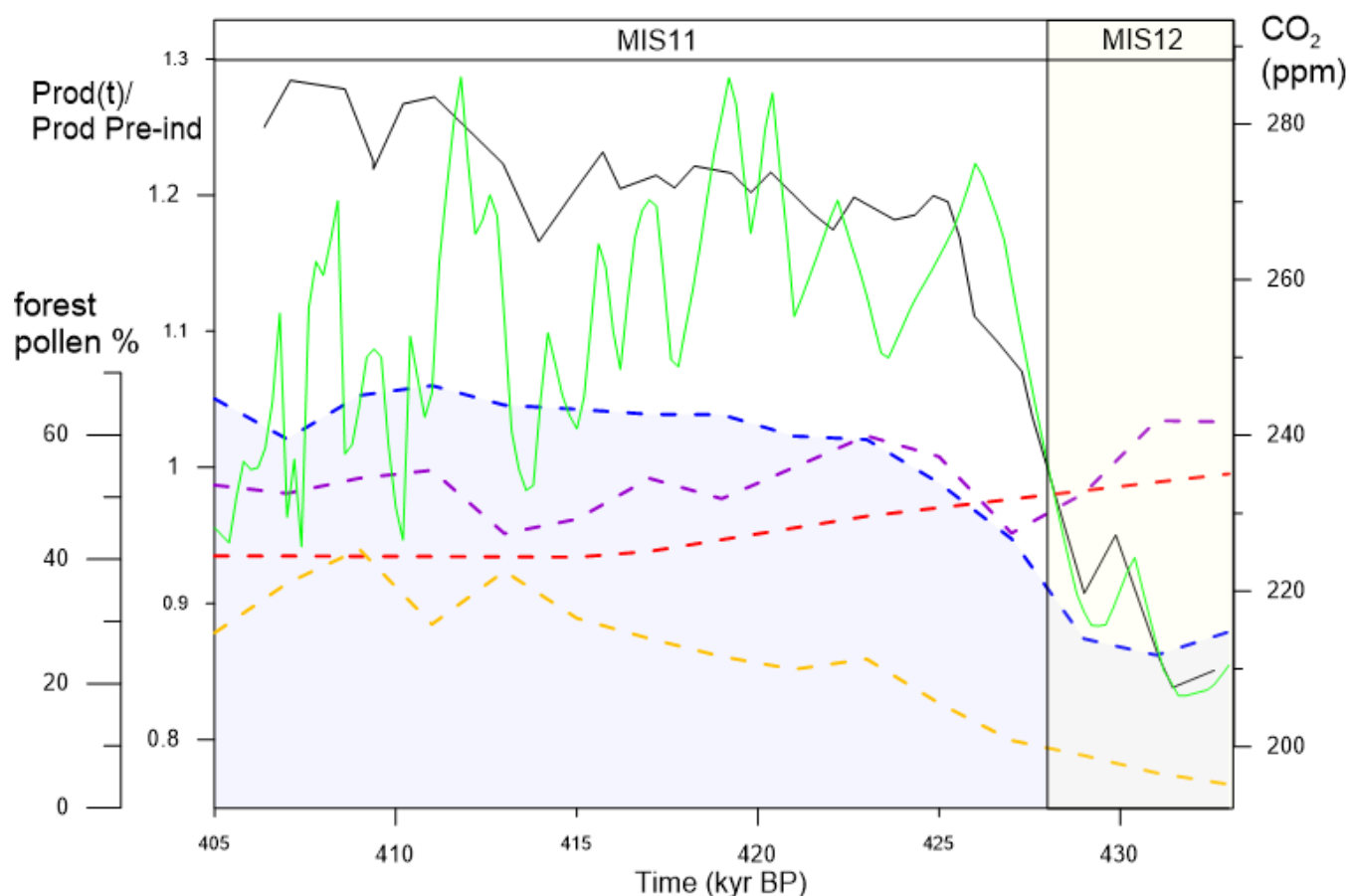
Figure 8: Comparison of forest pollen composites and observed global biosphere productivity (inferred from $\Delta^{17}O$ of O_2, solid green line,
485   Brandon et al. (2020)) and CO_2 (solid black line, Lüthi et al. (2008)) over TV. Forest pollen composites from Fig. 5 are shown in dashed blue (Eurasian), yellow (Mediterranean), purple (Tropical), red (South African) and black (Global mean) lines.

To further assess the carbon sink potential of temperate and boreal forests we analyze the variation of the simulated

490   total carbon stock (i.e carbon fluxes between the atmosphere and the {vegetation+soil} system), both a proxy for terrestrial

biosphere productivity and a direct measure of atmospheric CO_2 removal. Figure 9a represents the total simulated terrestrial carbon stock for four different zonally-averaged vegetation types following the pre-industrial Holocene biomes simulated by Prentice et al., 2011: temperate parkland and sclerophyll woodland ([-90:-30] °N), tropical forest ([-30:15] °N), warm-temperate forest and sclerophyll woodland ([15:40] °N) and high-latitude boreal and temperate forest ([40:90] °N). The

495 Southern forest group features very low and slightly growing carbon stocks (brown, Fig. 9a). On the contrary, the Tropical forest is the largest terrestrial carbon stock, accounting for approximately 50% of the total carbon stock (dark green, Fig. 9c) throughout the termination. The relatively strong increasing trend in carbon stocks (~8.1 GtC/kyr, Fig. 9a) is segmented in two parts: a steep carbon stock rise at the onset of MIS11 from 436 to 425 kyr BP and a smoother rise from 425 to 410 kyr BP. The Mid-latitude temperate forest represents around 20% of the total carbon stock (yellow, Fig. 9c). The slowly increasing

500 stock becomes very sharp at 416 kyr BP and peaks at 500 GtC around 411 kyr BP (Fig. 9a). Finally, the High-latitude boreal and temperate forest features the strongest mean increase in carbon stock (+13.7 GtC/kyr, light green, Fig. 9a) among all regions. We observe a steep rise until 425 kyr BP, along with the Tropical forest, giving way to a smoother trend. A second strong increase from 416 kyr BP leads to a peak value of 700 GtC at 409 kyr BP. This first rise can be linked to the synchronous biosphere productivity surge (Fig. 8).

505 While the total carbon stock increases by ~900 GtC until 410 kyr BP (Fig. 9c), Fig. 9b shows a redistribution of the carbon sinks mainly from the Tropical forests (~54% of total carbon stock at 436 kyr BP to ~45% at 404 kyr BP) to the high-latitude boreal and temperate forest (~20% of total carbon stock at 436 kyr BP to ~32% at 404 kyr bP) indicating a northward increase in carbon fluxes. Therefore, we argue that the high-latitude boreal and temperate forest account for the overall biosphere productivity increase (Fig. 8) leading to atmospheric CO_2 sequestration between 425 and 415 kyr BP.

510 Finally, the Tropical forest, the mid-latitude temperate forest and the high-latitude boreal and temperate forest are marked by a decreasing carbon stock from ~410 kyr BP resulting in a total carbon loss of 200 GtC in 404 kyr BP (Fig. 9b). We observe a similar decreasing trend in the biosphere productivity starting 3kyr earlier (Fig. 7) synchronous with increasing atmospheric CO_2 concentrations.
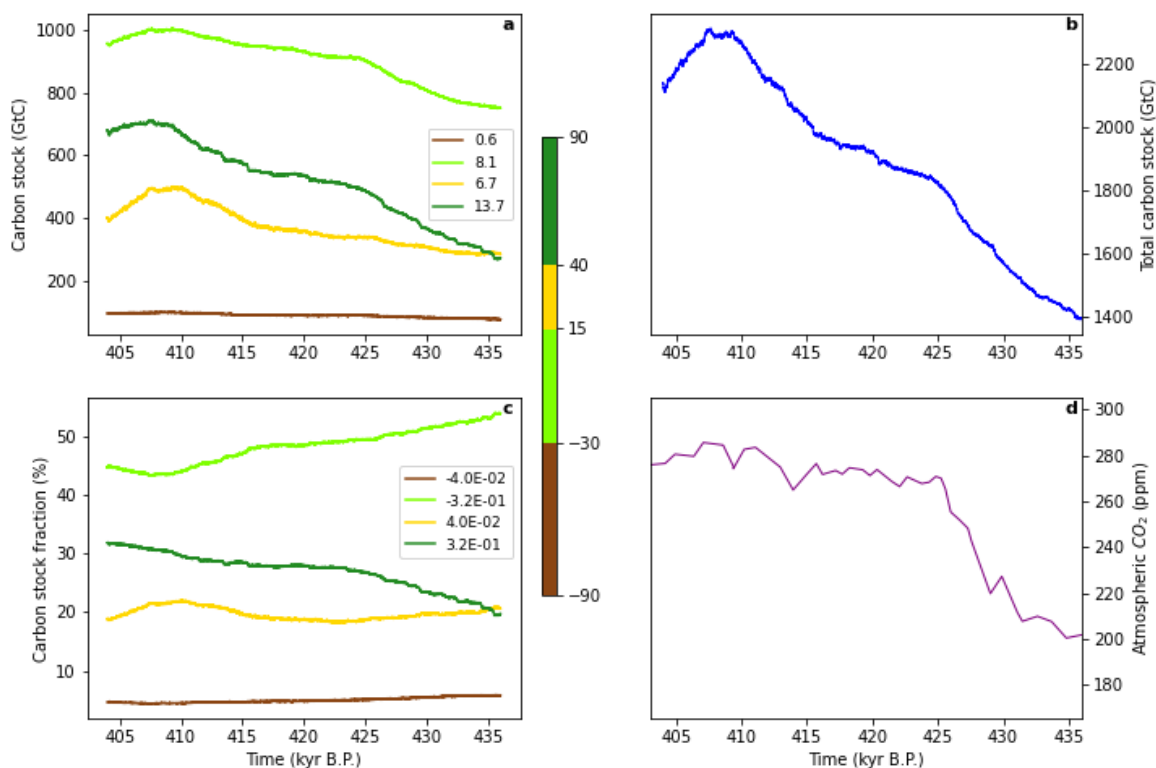
Figure 9: Zonal averages of simulated terrestrial biosphere a) carbon stock (GtC) and c) fraction of total carbon stocks (%) across TV. b) features the total carbon stock of simulated terrestrial biosphere and d) the atmospheric CO_2 concentration (from Lüthi et al., 2008). We estimate the terrestrial biosphere carbon stock as the sum of above- and below-ground carbon (e.g. green biomass + structural biomass + slow Soil Organic Matter (SOM) + fast SOM, Brovkin et al., 2002). The linear regression coefficient (GtC.kyr^{-1}) is provided for each time serie. Panel c) presents the total simulated terrestrial biosphere carbon stock (GtC) across TV.

5. Conclusion

Our new high-resolution pollen record (IODP U1386) is able to resolve submillennial changes of South-Iberian vegetation cover over TV. This sequence shows a moderate Mediterranean forest expansion during TV (maximum MF pollen percentage of ~50%) in line with seminal work by Oliveira, et al. (2016) and also unveils short timescale forest variations at the onset of the interglacial. TV is characterized by a two-step Mediterranean forest growth beginning at ~424 kyr BP lagging the marine isotopic interglacial (i.e. global ice volume decrease) by approximately 4 kyr.

At a global scale, we provide the first pollen record database for TV. Despite very sparse pollen data, we observe different forest developments varying with latitude and highlighting the strong increase of temperate and boreal forests across

the termination. We expect this new pollen database to open the way for an extensive comprehension of terrestrial biosphere-

530   climate interactions during TV. However, model-data comparisons remain essential to improve simulated forest accuracy in

order to achieve a global cover. Here we observe that iLOVECLIM simulated forests feature overall similar but weaker trends

than the pollen-based ones. This first assessment of global forest evolution during TV points out different driving mechanisms:

a strong impact of ice sheet retreat on forests is observed at high latitudes while lower latitude forests are probably more

influenced by precipitation and temperature changes (Yin & Berger, 2012).

535   Based on the presented global pollen-based vegetation records and simulation analysis we suggest the following:

1)   The strong warming at the onset of MIS11 results both in a strong increase of high latitude terrestrial biosphere
     productivity and in a rise in atmospheric CO_2 concentration probably driven by ocean physical and chemical
     degassing processes.

2)   Because of the exceptionally high ice sheet melt characterizing MIS11 (Dutton et al., 2015), forests can develop

540   northwards. This strong expansion, observed in the temperate and boreal forests, allows carbon removal by terrestrial
     biosphere to compensate the oceanic carbon losses, resulting in a long and unique CO_2 plateau from ~425 to ~415
     kyr BP.

We identify three major future research perspectives. First, a necessary step to achieve an accurate picture of terrestrial

545   biosphere evolution during TV is to increase the pollen record coverage, especially in poorly documented regions such as the

American continent, Siberia and central and southern Asia (tropical forests). Second, an integrated understanding of the carbon

cycle during TV will require both improving terrestrial biosphere simulations and taking into account the permafrost.

Increasing the number of PFTs and applying spatial downscaling methods should be considered to get precise terrestrial

biosphere representations. Finally, comparative studies of terrestrial biosphere-climate relations over contrasted terminations

550   such as TII may reveal successful in determining the specificity of TV. In this view, cooperation between the modelling and

observation communities becomes essential.

Data availability

The IODP U1386 pollen record and the resampled pollen database across Termination V documented here are available on

555   the PANGAEA data repository: *DOI number yet unavailable,* (Hes et al., 2021). Similarly, the iLOVECLIM output variables

(tree fraction and carbon stocks) presented here are available at: *Zenodo DOI number yet unavailable,* (Hes et al., 2021)

Competing interests

The authors declare that no competing interests are present.

560

10.5194/cp-2021-143
2021-11-01
Author(s) 2021. CC BY 4.0 License.

Acknowledgments

The present research used samples and data collected through the Integrated Ocean Drilling Program (IODP). We gratefully thank Déborah d'Olier and Ludovic Devaux for their precious contribution to U1386 pollen record analysis and Paul Moal for shedding light on the local depositional setting of U1386. We are also greateful to Josué M. Polanco-Martínez for his technical

565 advice in statistics. Similarly we appreciate Aurélien Quicquet and Didier Roche's help in manipulating the iLOVECLIM model. Special thanks to Amaelle Landais for her wise suggestions during result presentations. Finally we thank all cited authors for sharing their pollen data and warmly encourage more open data resources. This work was supported by the French ANR project NEANDROOTS n°CE27-0011-01.

570 **References**

Barth, Aaron M., Peter U. Clark, Nicholas S. Bill, Feng He, and Nicklas G. Pisias. "Climate evolution across the mid-brunhes transition." *Climate of the Past* (Copernicus GmbH) 14 (2018): 2071–2087.

Bartlein, P. J., et al. "Pollen-based continental climate reconstructions at 6 and 21 ka: a global
575 synthesis." *Climate Dynamics* (Springer Science and Business Media LLC) 37 (September 2010): 775–802.

Batchelor, Christine L., et al. "The configuration of Northern Hemisphere ice sheets through the Quaternary." *Nature Communications* (Springer Science and Business Media LLC) 10 (August 2019).

580 Bennett, K. D. "Psimpoll and pscomb: computer programs for data plotting and analysis." *Uppsala, Sweden: Quaternary Geology, Earth Sciences, Uppsala University. Software available on the internet at http://www. kv. geo. uu. se*, 2000.

Berger, AndréL. "Long-Term Variations of Daily Insolation and Quaternary Climatic Changes." *Journal of the Atmospheric Sciences* (American Meteorological Society) 35 (December 1978):
585 2362–2367.

Berger, Wolfgang H., and Gerold Wefer. "On the dynamics of the ice ages: Stage-11 paradox, mid-Brunhes climate shift, and 100-ky cycle." *GEOPHYSICAL MONOGRAPH-AMERICAN GEOPHYSICAL UNION* (AGU AMERICAN GEOPHYSICAL UNION) 137 (2003): 41–60.

Birks, H. J. B., and H. H. Birks. "Quaternary paleoecology: London." *Edward Arnold* 8 (1980): 289.

590 Bosmans, J. H. C., S. S. Drijfhout, Erik Tuenter, F. J. Hilgen, Lucas J. Lourens, and E. J. Rohling. "Precession and obliquity forcing of the freshwater budget over the Mediterranean." *Quaternary Science Reviews* (Elsevier) 123 (2015): 16–30.

Bouttes, Nathaëlle, D. M. Roche, V. Mariotti, and L. Bopp. "Including an ocean carbon cycle model into iLOVECLIM (v1. 0)." *Geoscientific Model Development* (Copernicus GmbH) 8 (2015):
595 1563–1576.

Bouttes, Nathaelle, Didier Swingedouw, Didier M. Roche, Maria F. Sanchez-Goni, and Xavier Crosta. "Response of the carbon cycle in an intermediate complexity model to the different climate configurations of the last nine interglacials." *Climate of the Past* (Copernicus GmbH) 14 (2018): 239–253.

600 Bouttes, Nathaëlle, et al. "Carbon 13 isotopes reveal limited ocean circulation changes between interglacials of the last 800 ka." *Paleoceanography and Paleoclimatology* (Wiley Online Library) 35 (2020): e2019PA003776.

Bradshaw, R. H. W., and Thompson Webb III. "Relationships between contemporary pollen and vegetation data from Wisconsin and Michigan, USA." *Ecology* (Wiley Online Library) 66
605 (1985): 721–737.

Brandon, Margaux, et al. "Exceptionally high biosphere productivity at the beginning of Marine Isotopic Stage 11." *Nature communications* (Nature Publishing Group) 11 (2020): 1–10.

Brovkin, Victor, Andrei Ganopolski, and Yuri Svirezhev. "A continuous climate-vegetation classification for use in climate-biosphere studies." *Ecological Modelling* (Elsevier) 101 (1997):
610 251–261.

Brovkin, Victor, et al. "Carbon cycle, vegetation, and climate dynamics in the Holocene: Experiments with the CLIMBER-2 model." *Global Biogeochemical Cycles* (American Geophysical Union (AGU)) 16 (December 2002): 86–1–86–20.

Castro, E. Blanco, et al. "Los Bosques Ibéricos, Barcelona." 1997.

615 Crowley, Thomas J. "Ice Age terrestrial carbon changes revisited." *Global Biogeochemical Cycles* (American Geophysical Union (AGU)) 9 (September 1995): 377–389.

Desprat, S., et al. "Is vegetation responsible for glacial inception during periods of muted insolation changes?" *Quaternary Science Reviews* (Elsevier) 24 (2005): 1361–1374.

Dupont, L. M., H. J. Beug, H. Stalling, and Ralf Tiedemann. "First palynological results from Site 658
620 at 21° N off Northwest Africa: Pollen as climate indicators. In Ruddiman, W., Sarnthein, M. et al." *Proceedings Ocean Drilling Program Scientific Results.* 1989. 93–112.

Dupont, Lydie M., and C. O. C. Agwu. "Latitudinal shifts of forest and savanna in NW Africa during the Brunhes chron: further marine palynological results from site M 16415 (9°; N 19° W)." *Vegetation History and Archaeobotany* (Springer) 1 (1992): 163–175.

625 Dupont, Lydie M., Fabienne Marret, and Kyaw Winn. "Land-sea correlation by means of terrestrial and marine palynomorphs from the equatorial East Atlantic: phasing of SE trade winds and the oceanic productivity." *Palaeogeography, Palaeoclimatology, Palaeoecology* (Elsevier) 142 (1998): 51–84.

Dupont, Lydie M., Thibaut Caley, J.-H. Kim, I. Castañeda, Bruno Malaizé, and Jaques Giraudeau.
630 "Glacial-interglacial vegetation dynamics in South Eastern Africa coupled to sea surface temperature variations in the Western Indian Ocean." *Climate of the Past* (Copernicus GmbH) 7 (2011): 1209–1224.

Dutton, Andrea, et al. "Sea-level rise due to polar ice-sheet mass loss during past warm periods." *science* (American Association for the Advancement of Science) 349 (2015).

635 Fawcett, Peter J., et al. "Extended megadroughts in the southwestern United States during Pleistocene interglacials." *Nature* (Nature Publishing Group) 470 (2011): 518–521.

Ganopolski, A., and R. Calov. "The role of orbital forcing, carbon dioxide and regolith in 100 kyr glacial cycles." *Climate of the Past* (Copernicus GmbH) 7 (2011): 1415–1425.

Goosse, Hugues, et al. "Description of the Earth system model of intermediate complexity LOVECLIM version 1.2." *Geoscientific Model Development* (Copernicus GmbH) 3 (2010): 603–633.

Govin, Aline, et al. "Persistent influence of ice sheet melting on high northern latitude climate during the early Last Interglacial." *Climate of the Past* (Copernicus GmbH) 8 (2012): 483–507.

Harris, Nancy L., et al. "Global maps of twenty-first century forest carbon fluxes." *Nature Climate Change* (Nature Publishing Group) 11 (2021): 234–240.

Hayashi, Ryoma, Takuya Sagawa, Tomohisa Irino, and Ryuji Tada. "Orbital-scale vegetation-ocean-atmosphere linkages in western Japan during the last 550 ka based on a pollen record from the IODP site U1427 in the Japan Sea." *Quaternary Science Reviews* (Elsevier) 267 (2021): 107103.

Heusser, Linda, and William L. Balsam. "Pollen distribution in the northeast Pacific Ocean." *Quaternary Research* (Elsevier) 7 (1977): 45–62.

Hoogakker, B. A. A., et al. "Terrestrial biosphere changes over the last 120 kyr." *Climate of the Past* (Copernicus GmbH) 12 (January 2016): 51–73.

Huntley, B. *An atlas of past and present pollen maps for Europe, 0-13,000 years ago.* Cambridge Cambridgeshire New York: Cambridge University Press, 1983.

Huntley, Brian. "European vegetation history: Palaeovegetation maps from pollen data - 13 000 yr BP to present." *Journal of Quaternary Science* (Wiley) 5 (1990): 103–122.

Johnson, Thomas C., et al. "A progressively wetter climate in southern East Africa over the past 1.3 million years." *Nature* (Nature Publishing Group) 537 (2016): 220–224.

Jouzel, Jean, et al. "Orbital and millennial Antarctic climate variability over the past 800,000 years." *science* (American Association for the Advancement of Science) 317 (2007): 793–796.

Juggins, S. "Package "rioja"–analysis of quaternary science data." *The Comprehensive R Archive Network*, 2009.

Kaboth, Stefanie, Bas de Boer, André Bahr, Christian Zeeden, and Lucas J. Lourens. "Mediterranean Outflow Water dynamics during the past˜ 570 kyr: Regional and global implications." *Paleoceanography* (Wiley Online Library) 32 (2017): 634–647.

Köhler, Peter, and Hubertus Fischer. "Simulating low frequency changes in atmospheric CO 2 during the last 740 000 years." *Climate of the Past* (Copernicus GmbH) 2 (2006): 57–78.

Landais, A., et al. "What drives the millennial and orbital variations of δ18Oatm?" *Quaternary Science Reviews* (Elsevier) 29 (2010): 235–246.

Lionello, Piero, et al. "The Mediterranean climate: an overview of the main characteristics and issues." *The Mediterranean climate: an overview of the main characteristics and issues.* Elsevier, 2006.

Lisiecki, Lorraine E., and Maureen E. Raymo. "A Pliocene-Pleistocene stack of 57 globally distributed benthic δ18O records." *Paleoceanography* (Wiley Online Library) 20 (2005).

Loughran, Tammas, et al. "Past and future climate variability uncertainties in the global carbon budget using the MPI Grand Ensemble." *Global Biogeochemical Cycles* (American Geophysical Union), 2021.

Loutre, Marie-France, and André Berger. "Marine Isotope Stage 11 as an analogue for the present interglacial." *Global and planetary change* (Elsevier) 36 (2003): 209–217.

Lüthi, Dieter, et al. "High-resolution carbon dioxide concentration record 650,000–800,000 years before present." *Nature* (Nature Publishing Group) 453 (2008): 379–382.

680 Maher Jr, Louis J. "Statistics for microfossil concentration measurements employing samples spiked with marker grains." *Review of Palaeobotany and Palynology* (Elsevier) 32 (1981): 153–191.

Masson-Delmotte, V., et al. Edited by T. Waterfield O. Yelekçi R. Yu J.B.R. Matthews and B. Zhou. *IPCC* (Cambridge University Press. In Press), 2021.

McManus, Jerry F., Delia W. Oppo, and James L. Cullen. "A 0.5-million-year record of millennial-
685 scale climate variability in the North Atlantic." *science* (American Association for the Advancement of Science) 283 (1999): 971–975.

Melles, Martin, et al. "2.8 million years of Arctic climate change from Lake El'gygytgyn, NE Russia." *science* (American Association for the Advancement of Science) 337 (2012): 315–320.

Moal-Darrigade, Paul, et al. "MOW strengthening and contourite development over two analog climate
690 cycles (MIS 12-11 and MIS 2-1) in the Gulf of Cadíz : an impact on North Atlantic climate during terminations and interglacials ?" *Global and Planetary Change*, 2021.

Morales-Molino, César, Ludovic Devaux, Muriel Georget, Vincent Hanquiez, and María F. Sánchez Goñi. "Modern pollen representation of the vegetation of the Tagus Basin (central Iberian Peninsula)." *Review of palaeobotany and palynology* (Elsevier) 276 (2020): 104193.

695 Oliveira, Dulce, et al. "The complexity of millennial-scale variability in southwestern Europe during MIS 11." *Quaternary Research* (Elsevier) 86 (2016): 373–387.

Overpeck, J., C. Whitlock, and B. Huntley. "Terrestrial biosphere dynamics in the climate system: past and future." In *Paleoclimate, global change and the future*, 81–103. Springer, 2003.

Peinado-Lorca, M., and J. M. Martínez-Parras. "Castilla-La Mancha." *La Vegetación de España*, 1987:
700 163-196.

Polunin, Oleg, and Martin Walters. *Guide to the Vegetation of Britain and Europe.* Oxford University Press, 1985.

Prentice, I. C., S. P. Harrison, and P. J. Bartlein. "Global vegetation and terrestrial carbon cycle changes after the last ice age." *New Phytologist* (Wiley) 189 (February 2011): 988–998.

705 Roche, D. M., H. Renssen, D. Paillard, and G. Levavasseur. "Deciphering the spatio-temporal complexity of climate change of the last deglaciation: a model analysis." *Climate of the Past* (Copernicus GmbH) 7 (June 2011): 591–602.

Roche, D. M., T. M. Dokken, Hugues Goosse, H. Renssen, and S. L. Weber. "Climate of the Last Glacial Maximum: sensitivity studies and model-data comparison with the LOVECLIM coupled
710 model." *Climate of the Past* (Copernicus GmbH) 3 (2007): 205–224.

Rodrigues, T., et al. "A 1-Ma record of sea surface temperature and extreme cooling events in the North Atlantic: A perspective from the Iberian Margin." *Quaternary Science Reviews* (Elsevier) 172 (2017): 118–130.

Rull, Valentí. "A note on pollen counting in palaeoecology." *Pollen et spores* 29 (1987): 471–480.

715 Sánchez Goñi, M. F., et al. "Tropically-driven climate shifts in southwestern Europe during MIS 19, a low eccentricity interglacial." *Earth and Planetary Science Letters* (Elsevier) 448 (2016): 81–93.

Sánchez Goñi, M.F., Frédérique Eynaud, Jean-Louis Turon, and N. J. Shackleton. "High resolution palynological record off the Iberian margin: direct land-sea correlation for the Last Interglacial complex." *Earth and Planetary Science Letters* (Elsevier) 171 (1999): 123–137.

720   Sánchez Goñi, María F., et al. "Pollen from the deep-sea: A breakthrough in the mystery of the Ice
         Ages." *Frontiers in plant science* (Frontiers) 9 (2018): 38.
      Shackleton, Nicholas J., Maria Fernanda Sánchez-Goñi, Delphine Pailler, and Yves Lancelot. "Marine
         isotope substage 5e and the Eemian interglacial." *Global and Planetary change* (Elsevier) 36
         (2003): 151–155.
725   Shukla, P. R., et al. "IPCC, 2019: Climate Change and Land: an IPCC special report on climate change,
         desertification, land degradation, sustainable land management, food security, and greenhouse
         gas fluxes in terrestrial ecosystems." (Intergovernmental Panel on Climate Change (IPCC))
         2019.
      Skinner, L. C., and N. J. Shackleton. "An Atlantic lead over Pacific deep-water change across
730   Termination I: implications for the application of the marine isotope stage stratigraphy."
         Quaternary Science Reviews (Elsevier) 24 (2005): 571–580.
      Stow, D. A. V., F. J. Hernández-Molina, C. Alvarez-Zarikian, and E. Scientists. "Expedition 339
         summary." *Proc. Ocean Drill. Prog* 339 (2013).
      Torres, Vladimir, Henry Hooghiemstra, Lucas Lourens, and P. Chronis Tzedakis. "Astronomical tuning
735   of long pollen records reveals the dynamic history of montane biomes and lake levels in the
         tropical high Andes during the Quaternary." *Quaternary Science Reviews* (Elsevier) 63 (2013):
         59–72.
      Tzedakis, P. C., Henry Hooghiemstra, and Heiko Pälike. "The last 1.35 million years at Tenaghi
         Philippon: revised chronostratigraphy and long-term vegetation trends." *Quaternary Science
740   Reviews* (Elsevier) 25 (2006): 3416–3430.
      Van Campo, Madeleine. "Relations entre la végétation de l'Europe et les températures de surface
         océaniques après le dernier maximum glaciaire." *Pollen et spores* 26 (1984): 497–518.
      Wagner, Bernd, et al. "Mediterranean winter rainfall in phase with African monsoons during the past
         1.36 million years." *Nature* (Nature Publishing Group) 573 (2019): 256–260.
745   Yin, Qiu Zhen, and André Berger. "Individual contribution of insolation and CO 2 to the interglacial
         climates of the past 800,000 years." *Climate dynamics* (Springer) 38 (2012): 709–724.
      Yin, Qiuzhen. "Insolation-induced mid-Brunhes transition in Southern Ocean ventilation and deep-
         ocean temperature." *Nature* (Nature Publishing Group) 494 (2013): 222–225.
      Zhao, Yan, et al. "Evolution of vegetation and climate variability on the Tibetan Plateau over the past
750   1.74 million years." *Science advances* (American Association for the Advancement of Science)
         6 (2020): eaay6193.

755